Relativistic correlation effects on the x-ray spectra of Li-like ions

L. Natarajan
Department of Physics, University of Mumbai, Mumbai 400098, India
(Received 17 November 2015; published 25 March 2016)

The wavelengths and rates of electric dipole transitions between states with $n = 2$ and $n = 1$ of doubly excited Li-like ions have been studied for some selected ions in the range $13 \leqslant Z \leqslant 54$ using fully relativistic multiconfiguration Dirac-Fock wave functions in the active space approximation with the inclusion of finite nuclear size, Breit interaction, self-energy, and vacuum polarization. A detailed discussion on the effects of intercomplex correlation around $Z = 26$ and intracomplex correlation around $Z = 37$ leading to irregularities and sharp discontinuities in the x-ray rates noticed for a few transitions has been provided. An unusually large contribution of Breit interaction has been found for intercomplex correlation in certain cases. The present results are compared with other available experimental and theoretical data. The errors associated with the transitions are highlighted for some experimentally available lines taking into account the uncertainties on the fine-structure energy levels and also on the line strengths.

DOI: 10.1103/PhysRevA.93.032516

I. INTRODUCTION

The spectral features of resonance and dielectronic satellite transitions in the inner shells of highly ionized atoms provide valuable information on the characteristics of hot plasmas such as electron temperature, density, and ionization balance [1,2] and are widely used in the modeling of astrophysical and laboratory induced plasmas. Hence precise experimental measurements and accurate theoretical data are crucial for unambiguous spectroscopic diagnostics. The energies and rates of $1s2lnl'$-$1s^2nl'$ and $1s^22l$ K x-ray satellites from highly charged few-electron ions have been investigated in laser produced plasmas [3–5], electron-beam ion traps [6–8], tokamak plasmas [9], and solar flares [10]. The $nln'l'$-$1sn'l'$ and $1s2lnl'$-$1s^2nl'$ ($n = 2,3$) spectral lines emitted from laser produced plasmas of two and three electron ions of elements in the range Na to V were observed by Aglitskii *et al.* [3]. Feldman *et al.*[4] have investigated the blended transitions from He- and Li-like ions for some light elements ranging from Na through Ti in laser produced plasmas and classified the spectral lines by comparison with *ab initio* intermediate coupling calculation that included relativistic effects and configuration interaction. The spectral line intensities from $1s2l3l'$-$1s^22l''$ transitions in Li-like ions have been shown to be sensitive to fluctuations in the electron density near the critical value for laser experiments [5]. The $1s^2nl$-$1s2pnl$ ($n = 2,3,4$) x-ray spectra in Li-like Ar were investigated in EBIT experiment [6] and also in TFR tokamak [9]. The measurements made on the satellite transitions from doubly excited $1s2l3l'$ and $1s3l3l'$ levels of Li-like and also from $1s^22l2l'$ of Be-like Ar on the Princeton Large Torus tokamak were reported by Beiersdorfer *et al.* and compared with Hebrew University Lawrence Livermore Atomic code (HULLAC) data [7]. Channel-specific dielectronic recombination cross sections for $1s2ln'l'$ ($n' = 2,3$) doubly excited levels of Li-like Kr were measured in EBIT experiment and compared with HULLAC data [8]. The synthetic $1snln'l'$-$1s^2nl$ x-ray satellite lines from Li-like Si were compared with solar flare spectra observed by the RESIK spectrometer on the CORONAS-F spacecraft [10].

The atomic data on the $1s^2nl$-$1s2pnl$ ($n = 2$ and 3) transitions in highly charged Li-like Fe were computed by Bely-Dubau *et al.* using SUPERSTRUCTURE code in intermediate coupling with relativistic corrections [11]. Following the same procedure, Bely- Dubau *et al.* reported atomic data from $1s^2nl$-$1s2l'nl$ transitions with $n = 2$ and 3 in Li-like Ca [12]. The radiative transitions from states of $1s2lnl'$ ($n = 2,3$, $l' = 1,2$) were calculated by Lihua *et al.* using Flexible Atomic code to analyze the spectrum from a photoionized Si plasma [13]. The modified Z expansion (MZ) calculations on the relative intensities of dielectronic satellite lines from $1s2l''nl'$-$1s^2n'l'$ (n,$n' = 2,3$) were reported by Safronova *et al.* for a wide range of Z [14]. The x-ray and Auger spectra for Li-like ions were studied by Chen using multiconfiguration Dirac- Fock (MCDF) wave functions in the extended average level scheme (EAL) with the inclusion of generalized Breit interaction and quantum electrodynamics corrections [15]. Extensive tabulations on the x-ray energies and rates for various transitions from $n = 2$ and 3 to$n = 1$ and the autoionization rates for doubly excited $2lnl'$ and $1s2lnl'$ states in ions with atomic numbers $Z = 6$–36 have been reported by Goryayev *et al.* [16]. The calculations were carried out by them using the modified Z expansion method with the inclusion of relativistic corrections within the framework of the Breit operator. Theoretical wavelengths and intensities of the dielectronic and inner-shell satellites of He-to C-like Fe, Li-like Ca, and Li-like S from three different methods (MZ, AUTOLSJ, and YODA) were compared with synthetic spectra by Kato *et al.* [17]. The weighted oscillator strengths and lifetimes for all experimentally known electric dipole transitions in Li-like S were calculated by Luna *et al.*[18] using the relativistic Hartree-Fock (HFR) model. However, these authors had not paid special attention to the irregular changes in the Z dependent characteristics of radiative transitions due to relativity, configuration interaction and level crossing.

We have recently reported our investigations on the effects of relativistic correlation on the normal $K\beta$ x-ray satellites [19] and on the special type of two-electron one-photon transitions [20] from states of $1s2s3p$ configuration in Li-like ions with $14 \leqslant Z \leqslant 54$ and made a detailed analysis on the

 ©2016 American Physical Society

irregular trend in the electric dipole ($E1$) line intensities for ions with $Z = 38$–43. In this work, we extend our experience in this field by investigating the fine structure states of 1s2p3s configuration in the Li-isoelectronic sequence with $13 \leqslant Z \leqslant 54$. The primary purpose of this paper is to analyze in detail the intracomplex correlation effects responsible for level crossing at around $Z = 37$, intercomplex correlation at around $Z = 26$ resulting in sharp discontinuity in the transition probabilities and also to investigate the influence of Breit interaction on the radiative transitions. To the best of our knowledge, the irregularities in the level structure along the Li-isoelectronic sequence due to strong inter- and intraconfiguration interactions have not been discussed in literature. The intracorrelation effects are noticed for ions with $Z > 36$ and the available data [15] are only for $Z = 42$. For ions around $Z = 26$, data are not reported for transitions where intercorrelation effects dominate except for Li-like Fe [11,15]. In the present work, we have made an attempt to make these available in print. The calculations are performed using MCDF wave functions with the inclusion of Breit interaction, self-energy and vacuum polarization. The finite nuclear size effect has been included in the calculations by considering a two-parameter Fermi charge distribution. The MCDF method which simultaneously treats both correlation and relativistic effects in the extended optimal level scheme (EOL) is shown to be efficient in treating the root collapsing effect [21] and also in treating the correlation effects due to strong interaction of the nearly degenerate excited states with the reference state [22]. The correlation effects have been computed by excitation of atomic orbitals in the active space approximation. The computations have been carried out using grasp2K code [23–25].

II. NUMERICAL PROCEDURE

In a multiconfiguration relativistic calculation, the configuration state functions (CSFs) are symmetry adapted linear combinations of Slater determinants constructed from a set of one-electron Dirac spinors. A linear combination of these configuration state functions (CSFs) is then used in the construction of atomic state functions (ASFs) with the same J and parity,

$$\Psi_i(J^P) = \sum_{\alpha=1}^{n_{\rm CSF}} c_{i\alpha}\Phi(\Gamma_\alpha J^P), \tag{1}$$

where $c_{i\alpha}$ are the mixing coefficients for the state i and n_{CSF} are the number of CSFs included in the evaluation of ASF. The Γ_α represents all the one-electron and intermediate quantum numbers needed to define the CSFs and the configuration mixing coefficients are obtained through the diagonalization of the Dirac-Coulomb Hamiltonian,

$$\mathbf{H}_{\rm DC} = \sum_i \left[c\alpha_i.\mathbf{p}_i + (\beta_i - 1)c^2 - \frac{Z}{r_i}\right] + \sum_{i<j}\frac{1}{r_{ij}}. \tag{2}$$

Once a set of radial orbitals and the expansion coefficients are optimized for self-consistency, Relativistic configuration interaction (RCI) calculations can be performed by including higher-order interactions in the Hamiltonian. The most important of these is the transverse photon interaction,

$$\mathbf{H}_{\rm trans} = -\sum_{i<j}^{N}\left[\frac{\alpha_i.\alpha_j\cos(\omega_{ij}r_{ij})}{r_{ij}} + (\alpha_i\cdot\nabla_i)(\alpha_j\cdot\nabla_j) \times\frac{\cos(\omega_{ij}r_{ij})-1}{\omega_{ij}^2 r_{ij}}\right], \tag{3}$$

where ω_{ij} is the wave number of the exchanged virtual photon and is obtained as the difference between the diagonal Lagrange multipliers associated with the orbitals. However, this is valid only when the shells are singly occupied and the diagonal energy parameters may not represent the correct binding energies of the orbitals in a variously ionized atomic system. Hence in the present work, the low-frequency limit $\omega_{ij} \rightarrow 0$ is considered and only the mixing coefficients are recalculated by diagonalizing the Dirac-Coulomb-Breit-Hamiltonian matrix. The dominant QED corrections comprise self-energy and vacuum polarization. While the former contribution is evaluated in the hydrogenlike approximation, the later correction is treated perturbatively. The theoretical background using relativistic wave functions and higher-order corrections is fully described in [23,26,27].

In the active space approximation method, the electrons from the occupied orbitals are excited to unoccupied orbitals in the active set. Since the orbitals with the same principal quantum number n have near similar energies, the active set is expanded in layers of n. Accurate level separation requires the inclusion of correlation through single and double (SD) excitations to CSFs with different orbitals. The correlation contribution was evaluated by considering SD excitations of electrons from the occupied shells to unoccupied virtual shells. In the first step, with no excitation we generated monoconfiguration wave functions for the $1s2p3s$ and $1s^23s$ reference configurations in EOL scheme using variational method. In EOL calculations, the radial functions and the mixing coefficients are determined by optimizing the energy functional, which is the weighted sum of the energy values corresponding to a set of $(2j+1)$ eigenstates. As this method is based on the simultaneous optimization of multiple levels with a selected J, the significant interactions between neighboring levels can be determined to near accuracy. In the second step, we considered limited admixture by allowing SD excitations of electrons in the reference configurations. In the third step, we included the $2s$ orbital and generated CSFs through SD excitations. In this step, only the $2s$ orbital was variational and all the other orbitals were frozen to their preceding optimization values. In the fourth step, we considered the $3p$ orbitals and followed a similar procedure as in the third step. Then, by gradually expanding the size of the active space in layers of n until the convergence and stability of the observable is obtained, the computations were repeated for each step by step multiconfiguration expansion taking care of the convergence criterion on the orbitals (10^{-8}). During each step of expansion, only the newly added orbitals were optimized and the active set considered in this work was $n = 1$–5 with sp symmetry. Though the EOL scheme yields accurate results, it also undergoes self-consistent field procedure convergence problems [28]. In the present study, wherever we encountered such a problem, we extended our

computations by including $6s,6p$ orbitals also so as to ensure that convergence of the calculated values is obtained. Further expansion of the active space did not contribute to the mixing coefficients. It may also be pointed out here that CSF expansion of the basis with ns and np orbitals with n ranging from 1 to 5 (or 6) may be construed as incomplete. Hence in order to check whether the introduction of CSFs with higher angular symmetry has any noticeable effects, especially for those ions exhibiting dramatic changes in the transition rates, we carried out calculations with SD excitation of orbitals with $n = 1$–7 active set for a few ions. While $n = 1$–6 set consisted of all orbitals with $l \leqslant n-1$, the $n = 7$ set was restricted to spd symmetry due to convergence problems. These calculations were performed on Li-like Ar, Fe, Kr, Zr, and Mo with a total of 549 and 5538 CSFs for the $1s^2 3s$ and $1s2p3s$ configurations respectively. However, it was noticed that these laborious calculations showed only marginal differences in the level energies and rates and hence we restricted our calculations only to sp orbitals.

III. RESULTS AND DISCUSSION

The three $J = 1/2$, three $J = 3/2$ and one $J = 5/2$ eigenstates of $1s2p3s$, barring strong configuration mixing can be uniquely identified on the basis of LSJ and jj coupling notations for low and high Z ions respectively. When a set of configurations such as $1s2p3s$, $1s2p3s + 1s2s3p$,...are included in the calculation, the Hamiltonian matrix is divided into noninteracting blocks of given parity and J. While expansion of the set with $n \geqslant 4$ improves the accuracy of the correlated functions, the strong contribution to mixing coefficients of the reference states are only from $1s2s3p$ and these two configurations put together give rise to six $J = 1/2$ odd parity eigenstates. At the high and low-Z limit, these six eigenstates can again be identified by their respective jj and LSJ labels. At intermediate Z, if the interaction is weak, then these states can still be labeled by the standard spectroscopic notation. However, as Z changes, the relative positions of energy levels change and that can lead to highly mixed configuration coefficients and when two or more such levels come close to each other, we come across complicated level crossing which can make identifying the energy levels consistently by their dominant jj or LSJ coefficients rather difficult. Under this description, states with the same nonrelativistic configuration will not cross each other. In the intermediate-Z region, some of the $1s2p3s$ and $1s2s3p$ states might contribute equally and then there is no clear-cut way of identifying these six levels by the dominant mixing coefficients in terms of jj or LSJ labels. In general, when such level crossings occur, energy ordering is used to assist with the classification. In the present work on $1s2p3s\ (^3P_1)\ ^2P_{1/2}$, we observe that even arranging the levels in the ascending order of energy may not help in unambiguously identifying the states.

It may be noted that the present usage of LSJ notation to classify the states is just a convenient way of labeling them even though it does not provide a good description especially for high Z ions and hence cannot be taken as a proper spectroscopic identification except for low Z ions. As reported in our previous paper on the level structure and the radiative decay of fine-structure states of $1s2s3p$ of Li-like ions [19], the energy ordering of the low-lying levels of $1s2p3s$ also does not follow a unique level scheme and with increasing Z, the levels are influenced differently by correlation and higher-order corrections. For example, the correlation effect makes $(^3P_1)\ ^2P_{1/2}$ of Fe more bound than $^4P_{5/2}$ and the respective MCDF energies are -453.3206 and -453.2936 a.u. However, Breit and QED effects interchange the ordering and the RCI energy eigenvalues of these two states are -453.1232 and -453.1405 a.u. leading to the normal LSJ structure. Similarly the MCDF energies of $^4P_{1/2}$ and $^4P_{3/2}$ of Mo are -1213.9949 and -1213.8003 a.u. respectively while with the inclusion of Breit and QED corrections, the respective energy values are -1212.9648 and -1213.0164 a.u. thereby flipping the ordering of these states.

The correlation CSFs that contribute substantially to the mixing coefficients of $1s2p(^3P_0)3s\ ^4P_{1/2}$ and $1s2p(^1P_1)3s\ ^2P_{1/2}$ states are mostly the same for all the ions investigated in this work and these two $J = 1/2$ states can still be conveniently identified by the dominant LSJ or jj components and energy ordering. However, for the $1s2p_{1/2}(^3P_1)3s\ J = 1/2$ state, we notice that for $Z \leqslant 36$ and $Z \geqslant 43$, it can be labeled by the relevant coupling schemes. For $Z \leqslant 36$, the first four CSF contributions to the $(^3P_1)\ ^2P_{1/2}$ are from $1s2p_{1/2}(^3P_1)3s$, $1s2s(^1S_0)3p_{1/2}$, $1s2p_{1/2}(^3P_0)3s$, and $1s2s(^3S_1)3p_{3/2}$ while for $Z = 54$, the last two CSFs listed above interchange and the states in descending order of contribution are $1s2p_{1/2}(^3P_1)3s$, $1s2s(^1S_0)3p_{1/2}$, $1s2s(^3S_1)3p_{3/2}$, and $1s2p_{1/2}(^3P_0)3s$. For $Z = 43$ and 44, the maximum contributing correlation states are $(^3P_1)\ ^2P_{1/2}$ and $(^3S_1)\ ^2P_{1/2}$ and the contributions from these two states add up to nearly 93%. However, for the ions with $Z = 37$–42, level crossing is encountered with two nearly degenerate levels. In our earlier analysis [19,20], we found that though the prominent mixing coefficient contribution to the ASF of $1s2s(^3S_1)3p_{3/2}\ J = 1/2$ should be from this state, it was only the second contributing state for ions with $Z = 38$–42. In this range, major contribution to $(^3S_1)\ ^2P_{1/2}$ was either from $1s2p_{1/2}(^3P_0)3s\ J = 1/2$ or from $1s2p_{1/2}(^3P_1)3s\ J = 1/2$ state and the expected $(^3S_1)\ ^2P_{1/2}$ became the second major contributor in both cases. In the present case, the level crossing and the restructuring of the spectrum is seen to be of a different nature. For both levels, the maximum contribution is from the same $(^3P_1)\ ^2P_{1/2}$ state. Naming them levels I and II, we find an irregular variation in the correlation strengths to these two levels. Ignoring the phase factor, the four significant mixing coefficients to the $(^3P_1)\ ^2P_{1/2}$ state (level I) are shown in Fig. 1. The differences in the correlation can thus well be attributed to the differences in how the electrons distribute themselves spatially and suggest how the most probable locations of the electrons can be severely affected by strong mixing.

In determining the accuracy of our computed data, we have considered a set of quality criteria such as optimization of the orbitals, convergence of the calculated term energies, comparison of the computed spectra with other available data, and agreement between the length and velocity forms of transition rates. The eigenvalues of the initial and final energy levels converged well for all the ions considered in this work. In Table I, sample data on the convergence of the MCDF energyeigen values for Li-like S with an increasing

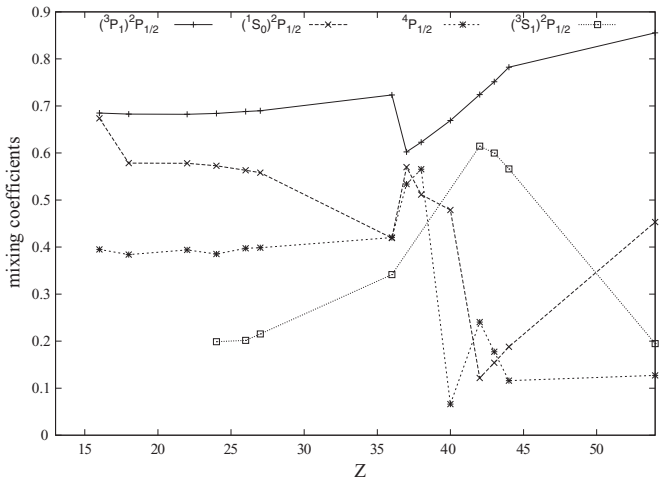

FIG. 1. Mixing coefficient admixture to the main $1s2p(^3P_1)3s\ ^2P_{1/2}$ state (level I).

set of correlation CSFs are given. Also listed in the table are the RCI term energies that include additional corrections from Breit interaction and QED effects. The active set in column 1 gives the orbitals in the set. For example, $\{n4,sp\}$ means that the set consists of all the orbitals with $n = 1$–4 with sp symmetry. All the energies listed in this table are bound-state negative values. It is seen from the table that the level energies converge well with the $\{n = 1$–$5,sp\}$ set.

In Table II, we compare the computed RCI wavelengths for 14 ions with the experimental values [3,4,6,9,29], SUPERSTRUCTURE values of Bely-Dubau *et al.* [11], relativistic EAL data of Chen [15], HFR value of Luna *et al.* [18], and modified Z expansion wavelengths of Goryayev *et al.* [16]. For $Z = 37$–42, the wavelengths from levels I and II are also reported. The RCI wavelengths for Al^{10+}, S^{13+}, and Fe^{23+} are in good agreement with the earlier experimental data [3,4,29] and differ by 0.4 Å for Ti^{19+} [29]. The present wavelength compares exceedingly well with the EBIT [6] measurement and differs marginally from the TFR value [9] for Ar^{15+}. The calculated wavelength for S^{13+} is in good agreement with the HFR value [18]. The difference between the present data and SUPERSTRUCTURE values of Bely-Dubau *et al.* for Fe^{23+} is mainly due to correlation and radiative corrections included in the present work. The RCI wavelengths are in very good agreement with the MCDF-EAL values of Chen [15] and also with the MZ data of Goryayev *et al.* [16] except for Li-like Al. The wavelengths from levels I and II for Zr^{37+}, Rb^{34+}, Sr^{35+}, and Mo^{39+} are nearly the same and differ by 0.001 Å. Figure 2 gives the Breit and QED corrections to the wavelengths of allowed and spin forbidden transitions. The contributions from these terms to the transition wavelengths exhibit a systematic variation with Z.

Our RCI calculations show that the ratios of length to velocity rates of the various transitions in general range 0.99–1.01 thereby supporting the accuracy of the calculated rates. In Table III, the computed RCI rates in length gauge are compared with the SUPERSTRUCTURE [11], HULLAC [8], MCDF-EAL [15], and MZ [16] rates. We noticed that for certain Z and certain transitions, our MCDF rates agree well with the earlier rates. As a sample case, our MCDF rate (3.27×10^{14} s^{-1}) for the $(^3P_1)^2P_{1/2}$-$^2S_{1/2}$ transition from Kr^{33+} is in agreement with the HULLAC (3.31×10^{14} s^{-1}) and MZ (3.22×10^{14} s^{-1}) rates whereas the RCI rate (2.638×10^{14} s^{-1}) differs by nearly 20%. The present rates for many transitions compare better with MZ rates [16] than with MCDF-EAL rates [15] especially for ions with $Z \leqslant 20$. The large correlation configurations along with the EOL scheme considered in this work might account for the deviations between our RCI and MCDF-EAL data [15]. The intensity of $^4P_{1/2}$-$^2S_{1/2}$ transition shows an irregular variation. It starts as a weak transition, peaks at $Z = 36$, experiences a sharp discontinuity at $Z = 37$ with a reduced intensity by an order of 2 and beyond this, its intensity again gradually increases. Similarly, the allowed transition from $(^3P_1)\,^2P_{3/2}$ also suffers strong irregularity. A sharp dip in line intensity occurs at Fe^{23+}. While the RCI rate for Fe^{23+} differs significantly from that of MCDF-EAL [15] rate, it compares well with the SUPERSTRUCTURE [11] value. This discontinuity in the intensity of the line from $(^3P_1)\,^2P_{3/2}$ at around $Z = 26$ is due to the abrupt changes in the admixture of intercomplex correlation. Our calculations show that $(^1P_1)\,^2P_{3/2}$ contributes to the mixing coefficient of $(^3P_1)\,^2P_{3/2}$ for the ions considered in this work except for ions with $Z = 26$–30. For example, the RCI mixing coefficient contributions from $(^1P_1)\,^2P_{3/2}$ to $(^3P_1)\,^2P_{3/2}$ are 15%, 7.7%, 4%, and 3% for Ar^{15+}, Ti^{19+}, Cr^{21+}, and Kr^{33+} respectively while for Fe^{23+} to Zn^{27+}, there is no admixture between these two states. Instead we notice that $1s2p3s\ ^4P_{3/2}$ contributes 2.8%, 2.7%, and 2.3% to $(^3P_1)\,^2P_{3/2}$ of Fe^{23+}, Co^{24+}, and Zn^{27+} respectively whereas we do not observe any contribution from this state to the rest of the ions. This sudden change in the intercomplex correlation reduces the $E1$ rate from this state at around

TABLE I. Energy eigenvalues in a.u. for the states of $1s2p3s$ configuration of Li-like S for increasing set of orbitals. All are bound state negative energies.

Active set	CSFs	$^4P_{1/2}$	$^4P_{3/2}$	$^4P_{5/2}$	$(^3P_1)\,^2P_{1/2}$	$(^1P_1)\,^2P_{1/2}$	$(^3P_1)\,^2P_{3/2}$	$(^1P_1)\,^2P_{3/2}$
DF	7	168.532 70	168.506 23	168.450 89	168.355 55	167.950 81	168.294 73	167.948 29
$\{1s2p3s\}$	16	168.528 42	168.501 82	168.446 65	168.322 69	167.195 99	168.267 30	167.911 78
$\{n23s\}$	32	168.529 43	168.502 83	168.447 63	168.325 34	167.925 15	168.269 45	167.917 84
$\{n3sp\}$	95	168.520 45	168.493 09	168.440 54	168.154 26	167.865 54	168.091 21	167.870 73
$\{n4sp\}$	251	168.525 99	168.498 75	168.446 18	168.185 74	167.884 89	168.119 89	167.890 68
$\{n5sp\}$	484	168.526 03	168.498 79	168.446 21	168.185 63	167.884 95	168.119 75	167.890 75
RCI	484	168.484 13	168.465 66	168.417 12	168.147 98	167.854 45	168.084 58	167.861 51

TABLE II. Comparison of RCI wavelengths in Å with other experimental (expt.) and theoretical (theor.) data. The values for transitions from the two $(^3P_1)\,^2P_{1/2}$ states for $37 \leqslant Z \leqslant 42$ are also included.

Z	$^4P_{1/2}$	$^4P_{3/2}$	$(^3P_1)\,^2P_{1/2}$		$(^1P_1)\,^2P_{1/2}$	$(^3P_1)\,^2P_{3/2}$	$(^1P_1)\,^2P_{3/2}$
13	7.842 62	7.841 67	7.820 15		7.782 28	7.817 90	7.781 68
G (theor.)		7.8315	7.7974		7.7727	7.7940	7.7735
A (expt.)					7.774		7.774
F (expt.)					7.773		
15	5.0817	5.0806	5.0627		5.0463	5.0592	5.0467
A (expt.)					5.0472		5.0472
L (theor.)					5.047		
F (expt.)					5.049		
G (theor.)	5.0804	5.0794	5.0616		5.0467	5.0581	5.0474
18	3.980 06	3.979 01	3.966 84		3.954 35	3.963 24	3.954 72
C (theor.)	3.9803	3.9793	3.9671		3.9551	3.9635	3.9558
G (theor.)	3.9793	3.9793	3.9661		3.9546	3.9626	3.9552
B (expt.)						3.9632	
T (expt.)						3.9628	
22	2.628 87	2.627 90	2.621 78		2.613 35	2.618 10	2.613 65
C (theor.)	2.6289	2.6280	2.6219		2.6136	2.6181	2.6140
G (theor.)	2.6284	2.6275	2.6214		2.6134	2.6178	2.6137
NIST (expt.)					2.243		
26	1.862 94	1.862 14	1.858 79		1.852 13	1.855 03	1.852 31
C (theor.)	1.8631	1.8624	1.8590		1.8523	1.8551	1.8523
G (theor.)	1.8628	1.8621	1.8587		1.8522		1.852 68
NIST (expt.)						1.8540	
Bely (theor.)	1.8625	1.8613	1.8582		1.8513	1.8543	1.8515
30	1.387 67	1.387 04	1.385 01		1.379 14	1.381 07	1.379 24
C (theor.)	1.3876	1.3870	1.3850		1.3791	1.3810	1.3792
G (theor.)	1.3874	1.3868	1.3847		1.3790		1.3791
36	0.953 09	0.952 64	0.951 61		0.946 24	0.947 37	0.946 24
C (theor.)	0.9530	0.9526	0.9516		0.9462	0.9473	0.9462
G (theor.)	0.952 74	0.985 234	0.951 29		0.946 11	0.947 22	0.946 08
37	0.901 41	0.900 27	0.900 70	0.899 34	0.894 02	0.895 00	0.894 01
38	0.853 04	0.852 02	0.852 43	0.851 19	0.845 90	0.846 87	0.845 88
40	0.767 15	0.766 31	0.766 70	0.765 66	0.760 43	0.761 26	0.760 41
42	0.693 39	0.693 44	0.693 02	0.692 14	0.686 97	0.687 68	0.686 93
C (theor.)	0.6934	0.6934	0.6921		0.6869	0.6877	0.6869
43	0.660 36	0.6605	0.6600		0.654 06	0.6547	0.6540
44	0.629 62	0.629 67	0.629 30		0.623 42	0.624 03	0.623 37
54	0.410 79	0.410 85	0.410 57		0.405 08	0.405 40	0.405 03

A: Laser produced plasma (Ref. [3]);
F: Laser produced plasma (Ref. [4]);
L: HFR (Ref. [18]);
B: EBIT (Ref. [6]);
T: TFR tokamak plasma (Ref. [7]);
NIST: (Ref. [29]);
Belly: SUPERSTRUCTURE (Ref. [11]);
C: MCDF-EAL (Ref. [15]);
G: MZ (Ref. [16]).

$Z = 26$, and drops drastically at $Z = 26$ beyond which it again starts increasing. The line intensity increases with Z for the rest of the allowed and spin forbidden $^4P_{3/2}$ - $^2S_{1/2}$ transitions. Considering $(^3P_1)\,^2P_{1/2}$ - $^2S_{1/2}$ transition from levels I and II, the rates show a discontinuity due to level crossing at $Z = 37$ for level I whereas a smooth increase in intensity with an increase in Z is observed for level II. The RCI rates for three selected transitions sensitive to strong configuration interaction are shown in Fig. 3. While the sharp dip around $Z = 26$ from $(^3P_1)\,^2P_{1/2}$ is due to the effect of intercomplex correlation, the other two discontinuities around $Z = 37$ are due to intracomplex correlation.

In Table IV, we analyze the effects of Breit interaction on the length gauge rates of allowed and intense $^4P_{3/2}$ - $^2S_{1/2}$ spin-forbidden transitions. The table gives the percentage contributions from this correction term to the MCDF rates. As evident from the table, the Breit interaction has quite different effects on different individual transitions. For certain Z, its contribution on some transitions is significant whereas for the others, it introduces a marginal change in

TABLE III. Comparison of RCI length gauge $E1$ rates in s^{-1} with other relativistic data. The transition rates from levels I and II of $(^3P_1)\,^2P_{1/2}$ for $37 \leqslant Z \leqslant 42$ are also included. The numbers in the square brackets are powers of 10.

Z	$^4P_{1/2}$	$^4P_{3/2}$	$(^3P_1)\,^2P_{1/2}$	$(^1P_1)\,^2P_{1/2}$	$(^3P_1)\,^2P_{3/2}$	$(^1P_1)\,^2P_{3/2}$
13	1.847[10]	5.676[10]	6.473[10]	2.865[13]	5.172[11]	2.817[13]
G		4.38[10]	3.61[12]	2.07[13]	2.45[12]	2.08[13]
16	1.258[11]	3.607[11]	1.097[13]	5.242[13]	6.059[12]	5.428[13]
G	1.2[11]	3.5[11]	9.28[12]	5.09[13]	4.39[12]	5.07[13]
18	3.82[11]	1.159[12]	1.816[13]	8.674[13]	7.282[12]	9.103[13]
G	3.63[11]	1.12[12]	1.59[13]	8.43[13]	4.63[12]	8.40[13]
C	3.42[11]	1.04[12]	1.44[13]	7.78[13]	4.58[12]	7.74[13]
22	2.343[12]	7.826[12]	4.236[13]	2.618[14]	4.937[12]	2.177[14]
C	2.13[12]	7.17[12]	3.67[13]	1.83[14]	2.54[12]	1.89[14]
G	2.21[12]	7.59[12]	3.93[13]	1.99[14]	2.66[12]	2.0[14]
26	9.687[12]	3.324[13]	8.084[13]	4.029[14]	3.401[10]	4.354[14]
C	8.84[12]	3.04[13]	7.84[13]	3.71[14]	3.98[11]	3.78[14]
G	9.08[12]	3.19 [13]	8.25[13]	4.05[14]		4.03[14]
B	6.10[12]	2.661[13]	7.564[13]	3.989[14]	3.0[10]	4.196[14]
30	3.035[13]	9.309[13]	1.421[14]	7.078[14]	1.211[13]	7.493[14]
C	2.79[13]	8.81[13]	1.46[14]	6.64[14]	3.97[12]	6.77[14]
G	2.94[13]	9.25[13]	1.52[14]	7.31[14]		7.36[14]
36	1.275[14]	2.537[14]	2.638[14]	1.422[15]	7.709[13]	1.427[15]
C	1.16[14]	2.53[14]	3.06[14]	1.36[15]	7.43[13]	1.35[15]
G	1.16[14]	2.72[14]	3.22[14]	1.53[15]	8.14[13]	1.51[15]
F			3.31[14]			
37	1.02[12]	2.818[14]	1.589[14] 2.891[14]	1.581[15]	9.304[13]	1.571[15]
38	1.762[12]	3.053[14]	1.976[14] 3.234[14]	1.749[15]	1.114[14]	1.723[15]
40	6.91[12]	3.335[14]	3.011[14] 3.898[14]	2.126[15]	1.507[14]	2.065[15]
42	2.746[13]	5.465[14]	4.421[14] 4.387[14]	2.554[15]	2.01[14]	2.445[15]
C	1.47[13]	4.74[14]	5.12[14]	2.46[15]	1.91[14]	2.36[15]
43	4.796[13]	6.756[14]	5.314[14]	2.796[15]	2.28[14]	2.66 [15]
44	7.86[13]	8.198[14]	6.294[14]	3.046[15]	2.6[14]	2.882[15]
54	9.236[14]	2.83[15]	1.825[15]	6.647[15]	7.234[14]	6.026[15]

B: SUPERSTRUCTURE (Ref. [11]);
C: MCDF-EAL (Ref. [15]);
G: MZ (Ref. [16]);
F: HULLAC (Ref. [9]).

the rates. The Breit interaction reduces the rates of allowed transitions from $(^1P_1)\,^2P_{1/2}$ and $(^1P_1)\,^2P_{3/2}$ states and enhances the rates from $(^3P_1)^2P_{3/2}$ and $^4P_{3/2}$ states. An unexpected large contribution of Breit interaction has been observed for

TABLE IV. The contributions from Breit interaction in percentage to the electric dipole allowed and spin-forbidden transitions from states of $1s2p3s$ configuration.

Z	$^4P_{1/2}$	$^4P_{3/2}$	$(^3P_1)\,^2P_{1/2}$	$(^1P_1)\,^2P_{1/2}$	$(^3P_1)\,^2P_{3/2}$	$(^1P_1)\,^2P_{3/2}$
13	17.86	19.62	− 4.65	− 0.14	9.60	− 0.31
15	34.3	19.6	9.59	− 2.01	6.9	− 1.27
18	39.13	17.73	10.43	− 2.32	8.82	− 1.61
22	40.0	16.18	11.13	− 2.59	10.73	− 1.58
26	44.9	12.22	7.12	− 2.71	3300	− 1.86
30	49.5	10.16	− 1.82	− 2.78	33.85	− 2.54
36	48.8	5.86	− 19.37	− 2.87	24.38	− 3.45
37	− 68.32	4.76	17.13(I), -21.51(II)	− 4.62	23.32	− 3.62
38	− 64.47	3.79	45.59(I), -21.56(II)	− 2.81	21.87	− 3.74
40	− 37.4	0.45	39.01(I), -21.56(II)	− 2.92	23.31	− 4.19
42	18.9	11.88	26.79(I), -14.59(II)	− 2.80	18.42	− 4.01
43	54.2	11.08	21.97	− 2.38	19.11	− 4.08
44	92.79	9.9	15.38	− 8.45	18.56	− 4.25
54	340	3.70	− 9.26	− 2.56	15.61	− 4.35

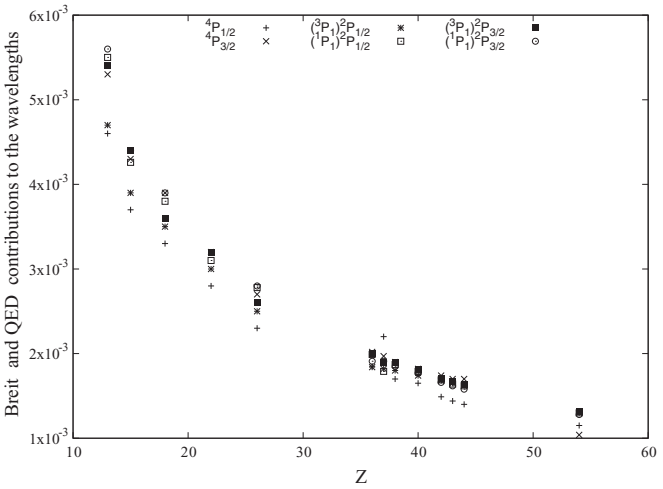

FIG. 2. Breit + QED contributions to the wavelengths in A^0 of the fine-structure transitions from states of $1s2p3s$ to $1s^23s(^2S_{1/2})$.

intercomplex correlation and a sixfold enhancement in the rate for transition from $(^3P_1)^2P_{3/2}$ of Fe^{23+} has been found. While Breit interaction enhances the transition rates from level I, it reduces the rates from level II. The contribution from Breit interaction to $^4P_{1/2}$ - $^2S_{1/2}$ is seen to be significant. Breit interaction considerably affects the level crossing interactions and reduces the rates. For Xe^{51+}, the contribution from Breit interaction is substantial. This is due to the fact that Breit interaction leads to a strong configuration mixing between $^4P_{1/2}$ and $(^3P_1)^2P_{1/2}$ states. The MCDF calculation shows a contribution of 7% from $(^3P_1)^2P_{1/2}$ to the mixing coefficient of $^4P_{1/2}$ and with Breit interaction included in the calculation, its contribution shoots up to 30%.

As an additional check on the reliability of the reported data, we calculated the transition rates using available experimental wavelengths and computed line strengths. The percentage difference δS between the length (S_l) and velocity (S_v) forms of line strengths are calculated relative to the average of S_l and S_v. δE is the difference between the experimental and

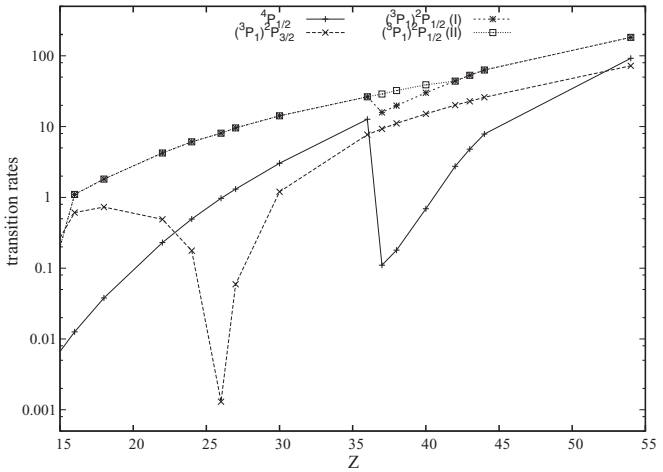

FIG. 3. Electric dipole transition rates in 10^{13} s^{-1} from $^4P_{1/2}$, $(^3P_1)^2P_{3/2}$, $(^3P_1)^2P_{1/2}$ (level I) and $(^3P_1)^2P_{1/2}$ (level II) of $1s2p3s$ to $1s^23s(^2S_{1/2})$.

TABLE V. The errors in computed wavelengths, line strengths, and rates for electric dipole transitions. $\delta\lambda$ listed for each element corresponds to the wavelength difference between our computed and experimental data. δS gives the % deviation in the length and velocity forms line strengths relative to average of S_l and S_v and δA is the % error between the RCI rates in length form and the energy scaled rates calculated with the average of S_l and S_v. The numbers within the brackets denote powers of 10.

	% Error		
	$1s2p(^1P_1)3s$		$1s2p(^3P_1)3s$
Property	$^2P_{1/2}$	$^2P_{3/2}$	$^2P_{3/2}$
	$Z = 13$		
$\delta\lambda$	$+8.28(-3)$[a]	$+7.70(-3)$[a]	
	$+9.28(-3)$[b]		
δS	$-1.40(-1)$	$-1.69(-1)$	
δA	$-4.88(-1)$[a]	$-4.61(-1)$ [a]	
	$-4.90(-1)$[b]		
	$Z = 15$		
$\delta\lambda$	$-9.00(-4)$[a]	$-5.00(-4)$[a]	
	$-2.70\ (-3)$[b]		
δS	$-3.16(-1)$	$-3.60(-1)$	
δA	$-1.14(-1)$[a]	$-7.36(-2)$[a]	
	$-1.14(-1)$[b]		
	$Z = 18$		
$\delta\lambda$			$+4.00(-5)$[c]
			$+4.40(-4)$[d]
δS			-1.03
δA			-1.04[c]
			-1.06[d]
	$Z = 22$		
$\delta\lambda$	$+3.70(-1)$[e]		
δS	$-3.37(-1)$		
δA	-22.20[e]		

[a]Reference [3].
[b]Reference [4].
[c]Reference [6].
[d]Reference [9].
[e]Reference [29].

calculated wavelengths. With A as the RCI rate and A' as the rate calculated using the observed wavelengths and computed line strengths, the uncertainty with respect to our computed rate is (δA). In calculating A', we have used the average of S_l and S_v. The uncertainty estimates δE, δS, and δA are listed in Table V. The relative error in the transition wavelengths is marginal except for Ti^{19+}. The relative difference in the length and velocity forms of line strengths is within a fraction of a percent except for Ar^{15+} which is 1%. As seen from Table III, our RCI wavelength for $(^1P_1)$ $^2P_{1/2}$ - $^2S_{1/2}$ agrees extremely well with the earlier relativistic data [15,16]. However all these theoretical wavelengths differ considerably from NIST data [29] and this difference in wavelength accounts for the 22% error in transition rate.

IV. CONCLUSION

Wavelengths and rates for the electric dipole transitions from the fine-structure states of $1s2p3s$ configuration in ions

of the Li-isoelectronic sequence have been calculated using the RCI method. The Z and transition dependence of Breit interaction on the transition rates is analyzed in detail. The level-crossing configuration interaction causes complications in the behavior of transition rates. Some irregularities and sharp discontinuities in the rates are noticed for a few transitions either due to intracomplex level crossing interactions or due to intercomplex correlation effect and this perturbs the systematics of the transition rates along the Li-isoelectronic sequence thereby confirming that the interpolation of the transition rates cannot be used to predict the results within the sequence. Though elaborate treatment of the configurational mixing near the level crossings is needed for a thorough understanding of electron correlation [30], we expect that the two configuration approximation will provide some insight into intra- and interelectron correlations. The contribution of Breit interaction on the most intense transitions is marginal whereas a very large contribution has been found in certain cases. While level I shows a small reduction in rate for $Z = 37$ and 38, the rates from level II increase smoothly with Z. However, the differences in the rates are not large. Hence, with a marginal difference in the level energies and acceptable variations in the transition rates, unique identification of $(^3P_1)$ $^2P_{1/2}$ becomes rather difficult. The calculated results are supplemented with error estimates wherever possible.

ACKNOWLEDGMENTS

The author acknowledges the support from the Department of Science and Technology- Science and Engineering research Board (DST-SERB), Government of India under Project No. SR/S2/LOP-5/2012.

[1] H. R. Griem, *Principles of Plasma Spectroscopy* (Cambridge University Press, New York, 1997).
[2] A. H. Gabriel, Mon. Not. R. Astron. Soc. **160**, 99 (1972).
[3] E. V. Aglitskii, V. A. Boiko. S. M. Zakharov, S. A. Pikuz, and A. fa. Faenov, Sov. J. Quantum Electron **4**, 500 (1974).
[4] U. Feldman, G. A. Doschek, D. J. Nagel, R. D. Cowan, and R. R. Whitlock, Astrophys. J. **192**, 213 (1974).
[5] F. B. Rosmej, A. Calisti, B. Talin, R. Stamm, W. Süß, M. Geißel, D. H. H. Hoffmann, A. Ya. Faenov, and T. A. Pikuz, J. Quant. Spectrosc. Radiat. Transfer **71**, 639 (2001).
[6] C. Beiedermann, R. Radtke, and K. Fournier, Nucl. Instrum. Methods Phys. Res. B **205**, 255 (2003).
[7] P. Beiersdorfer, A. L. Osterheld, T. W. Phillips, M. Bitter, K. W. Hill, and S. von Goeler, Phys. Rev. E **52**, 1980 (1995).
[8] T. Fuchs, C. Biedermann, R. Radtke, E. Behar, and R. Doron, Phys. Rev. A **58**, 4518 (1998).
[9] TFR group, F. Bombarda, F. Bely-Dubau, P. Faucher, M. Cornille, J. Dubau, and M. Loulergue, Phys. Rev. A **32**, 2374 (1985).
[10] K. J. H Phillips, J. Dubau, J. Sylwester, and B. Sylwester, Astrophys. J. **638**, 1154 (2006).
[11] F. Bely-Dubau, A. H. Gabriel, and S. Volonté, Not. R. Astron. Soc. **186**, 405 (1979).
[12] F. Bely Dubau *et al.*, Mon. Not. R. Astron. Soc. **201**, 1155 (1982).
[13] B. Lihua, Z. Wu, Duan Bin, Y. Ding, and J. Yan, Phys. Plasmas **18**, 023301 (2011).
[14] U. I. Safranova, M. S. Safronova, and R. Bruch, J. Phys. B **28**, 2803 (1995).
[15] M. H. Chen, At. Data. Nucl. Data Tables **34**, 301 (1986).
[16] F. F. Goryayev, A. M. Urnov, and L. A. Vainshtein, arXiv:physics/0603164.
[17] T. Kato, U. I. Safronova, A. S. Shlyapiseva, M. Cornille, J. Dubau, and J. Nilsen, At. Data Nucl. Data Tables **67**, 225 (1997).
[18] F. R. T. Luna, A. J. Mania, and J. A. Hernandes, J. Appl. Spectrosc. **76**, 447 (2009).
[19] L. Natarajan, A. Natarajan, and R. Kadrekar, Phys. Rev. A **82**, 062514 (2010).
[20] L. Natarajan, Phys. Rev. A **88**, 052522 (2013).
[21] J. Bieron, I. P. Grant, and C. F. Fischer, Phys. Rev. A **56**, 316 (1997).
[22] L. Natarjan and A. Natarjan, Phys. Rev. A **75**, 062502 (2007).
[23] F. A. Parpia, C. Froese Fischer, and I. P. Grant, Comput. Phys. Commun. **94**, 249 (1996).
[24] P. Jonsson, X. He, C. Froese Fischer, and I. P. Grant, Comput. Phys. Commun. **177**, 597 (2007).
[25] P. Jonsson, G. Gaigalas, J. B. Bieron, C. Froese Fischer, and I. P. Grant, Comput. Phys. Commun. **184**, 2197 (2013).
[26] B. J. Mckenzie, I. P. Grant, and P. H. Norrington, Comput. Phys. Commun. **21**, 233 (1980).
[27] I. P. Grant, *Relativistic Quantum Theory of Atoms and Molecules: Theory and Computation* (Springer, New York, 2007).
[28] R. Gebarowski, J. Migdalek, and J. R. Bieron, J. Phys. B, At. Mol. Opt. Phys. **27**, 3315 (1994).
[29] Online bibliographic database at NIST, http://physics.nist.gov/asd3.
[30] I. I. Sobelman, *Atomic Spectra and Radiative Transitions* (Springer-Verlag, Berlin, 1991).